Water Research 197 (2021) 117092

Contents lists available at ScienceDirect

Water Research

journal homepage: www.elsevier.com/locate/watres

Electrogenic and hydrocarbonoclastic biofilm at the oil-water interface as microbial responses to oil spill

Emilio D'Ugo[a,*], Lucia Bertuccini[b], Francesca Spadaro[b], Roberto Giuseppetti[a], Francesca Iosi[b], Fabio Santavenere[c], Fausto Giuliani[c], Massimo Gricia[c], Andrea Rodomonte[d], Nicola Lovecchio[e], Arghya Mukherjee[f], Paola Bucci[a], Milena Bruno[b], Emilia Stellacci[g], Antonietta Bernardo[h], Fabio Magurano[a]

[a] Department of Infectious Diseases, Istituto Superiore di Sanità, Rome, Italy
[b] Core Facilities, Istituto Superiore di Sanità, Rome, Italy
[c] National Center for Innovative Technologies in Public Health, Istituto Superiore di Sanità, Rome, Italy
[d] National Centre for the Control and Evaluation of Medicines, Istituto Superiore di Sanità, Rome, Italy
[e] Department of Information Engineering, Electronics and Telecommunications, Sapienza University of Rome, Rome, Italy
[f] Centre for Genetic Engineering and the Department of Biotechnology, University of Calcutta, Kolkata, India
[g] Department of Oncology and Molecular Medicine, Istituto Superiore di Sanità, Rome, Italy
[h] National Center for Research and Preclinical and Clinical Evaluation of Drugs, Istituto Superiore di Sanità, Rome, Italy

ARTICLE INFO

Article history:
Available online 27 March 2021

ABSTRACT

The oil-water interface formed during an oil spill represents a challenging environment for pelagic communities living in aquatic ecosystems. At this anoxic barrier, we report the formation of a microbial hydrocarbonoclastic biofilm capable of electron transfer along the water column. This biofilm generated a membrane of surface-active compounds that allowed the spontaneous separation of electrical charges, causing the establishment of an anodic and a cathodic region and, as a result, the spontaneous creation of a liquid microbial fuel cell. Such floating biofilm was connected to the water column underneath by floating filaments that could contribute to oxygen reduction at distance. The filaments revealed an unusual lipid content induced by anoxic conditions, with prominent ultrastructural features similar to myelin found in oligodendrocytes of the vertebrate nervous system. Furthermore, these filaments showed an interesting cross-reactivity towards different epitopes of the myelin basic protein (MBP) and Claudin 11 (O_4) of human oligodendrocytes. The presence of a network of filaments similar to myelin suggests the probable existence of evolutionary connections between very distant organisms. Collectively these results suggest a possible mechanism for how lake microbial communities can adapt to oil spills while offering an interesting starting point for technological developments of liquid microbial fuel cells related to the study of hydrocarbon-water interfaces.

The data that support the findings of this study are openly available in figshare at https://figshare.com/s/72bc73ae14011dc7920d.

1. Introduction

Massive oil spills in natural waters have an immediate effect on oxygen levels in the water bodies due to the reduction in atmospheric gaseous exchange and lowered availability of light for phytoplankton, especially in the euphotic zone (Williams and Mann, 2020). Additionally, oxygen under the water surface is consumed by microbial oxidation processes with a consequent slowdown in the degradation of hydrocarbon substances (Atlas, 1995). Although in these circumstances successional microbial communities of facultative aerobic or anaerobic hydrocarbonoclastic species can complete this degradation (Hazen et al., 2010; Gutierrez et al., 2016), the creation of a zonal anoxic barrier in the ecosystem niches represents a challenge for oxygenotrophic species that must complete their oxidative processes.

Bacterial biofilms are three-dimensional structures that usually grow adherent to abiotic or biotic surfaces and represent an

* Corresponding author.
E-mail address: emilio.dugo@iss.it (E. D'Ugo).

https://doi.org/10.1016/j.watres.2021.117092

emerging issue in all environments (Flemming et al., 2016). Creating biofilm communities at oil spill sites could be a way to improve the microorganism's planktonic life. Moreover, the matrix biofilm determines an efficient milieu for hydrocarbon degradation, wherein microbes are capable of protecting themselves from environmental stress and enhances their ability to adapt (Decho, 2000).

The biofilm growth, beneath hydrocarbon substances, seems to be associated with the ability of these bacteria to detect, at the level of the hydrocarbon-water interface, the bioavailability of nutrients, which constitute a source of carbon and energy (Klein et al., 2010).

Although the existence of biofilm at the hydrocarbon-water interface is documented (Klein et al., 2010), there is currently no experimental evidence on how these aquatic communities are structured to cope with the anoxic barriers that are usually produced during hydrocarbon degradation. Moreover, it is not known how hydrocarbonoclastic biofilms can organize themselves to guarantee the flow of energy from the oil-water interface to the water column.

The aim of this study was to study the microbiome and ex situ response of a lake microbial community and its adaptations under conditions of hydrocarbon spills. In the present study, we have demonstrated the formation of a hydrocarbonoclastic and electrogenic biofilm with filamentous bacteria along water column during oil spills where a putative electrical conduction system antigenically and ultrastructurally similar to myelin can be observed. Additionally, a new method for developing Liquid Microbial Fuel Cells (L-MFCs) has also been described.

2. Material and methods

2.1. Sampling site and sample processing

Sampling was performed in Pertusillo Lake, an artificial reservoir situated in the territories of Grumento Nova, Montemurro and Spinoso towns, Basilicata region (Southern Italy). Different samples were collected three months after the oil spill and from dinoflagellate algal blooms which occurred in February 2017 (European Parliament, 2017; ARPAB, 2017). The samples were stored in iceboxes, transported to the laboratory and immediately processed following an ultrafiltration protocol as previously described (D'Ugo et al., 2016). Sequencing data was submitted to the NCBI Sequence Read Archive (SRA) (BioProject accession number PRJNA412797). For this study, we selected the sample 1B (Total Hydrocarbon Content of 900 µg/L and algal bloom of *Peridinium sp* 10^6 cells/ mL; (ARPAB, 2017), taken from Madonna Grumentina (N 40.29172, E 15.92957) on May 22, 2017, just under the water surface. The retentate (50 ml) was aliquoted and used for laboratory investigations.

2.2. Culture media and fuels

Freshwater salts solution (M9) was prepared as previously described (Notomista et al., 2011) without adding sea salts. After autoclaving, 5 ml of sterile trace element solution was added to each liter of cooled water. The trace element solution contained: 30.1 g/L $MgSO_4$, 27.3 g/L $FeSO_4$ x $7H_2O$, 5.4 g/L MgO, 1.0 g/L $CaCO_3$, 0.72 g/L $ZnSO_4 \times 7\ H_2O$, 0.56 g/L $MnSO_4 \times H_2O$, 0.125 g/L $CuSO_4 \times 5\ H_2O$, 0.14 g/L $CoSO_4 \times 7\ H_2O$, 0.03 g/L H_3BO_3, 0.004 g/L $NiCl_2 \times 6\ H_2O$,0.006 g/L $Na_2MoO_4 \times 2\ H_2O$ and 25.6 mL/L HCl (36%). As an alternative to M9, source water (here called AR9) was purchased by Aretina Acque Minerali (S.N.C., Florence, Italy), filtered with a 0.1 µm filter (Sartorius, Italy) and autoclaved. Car diesel oil was purchased from IP (GO – Diesel Plus, Italiana Petroli), and Q8 (Kuwait Petroleum Italia) and filtered with 0.2 µm filter. Tests were performed as suggested by the European Pharmacopoeia and reported elsewhere, to assess sterile conditions (European Pharmacopoeia, 2014; D'Ugo et al., 2018).

2.3. Microcosms and biofilms formation in diesel

Five ml of filtered environmental sample 1B was enriched in 50 ml of Luria-Bertani (LB) broth for a week at 30°C (1B_LB). The culture was centrifuged at 6000 rcf for 10 min at room temperature (RT) and washed twice with M9 to remove all traces of residual carbon source. The pellets of sample 1B_LB were resuspended in M9 and estimated using a spectrophotometer at 600 nanometers (nm) (SPECTROSTAR nano, BMG LABTECH,Germany). One optical density (OD) of sample 1B_LB was inoculated in 50 mL tubes (Falcon) with 30-40 mL of M9 supplemented with trace elements (5ml/L) and 10% of diesel as a sole energy source for six months at 30°C (sample 1B_LB_D). To study growth under different nutritional conditions, microcosms derived from sample 1B_LB were supplemented with LB and 10% of diesel oil and incubated at 30°C. Ten milliliters of samples were pelleted and resuspended in 1 mL M9 to evaluate growth; optical density (OD) measurments were recorded at 600 nm using a spectrophotometer (SPECTROSTAR nano, BMG LABTECH, Germany).

2.4. Isolation of total microbiome DNA and high throughput 16S rRNA gene sequencing

Genomic DNA (gDNA) from 1B, 1B_LB and 1B_LB_D samples were extracted with NucleoSpin Tissue(®) Kit, (Macherey-Nagel, Germany) as instructed by the manufacturer and quantified with a spectrophotometer (NanoDrop, Thermo Fisher). High throughput sequencing of V3-V4 and V3-V5 regions of the 16S rRNA gene for the microbiome was performed by Eurofins MWG Operon (Ebersberg, Germany). Sequencing data was submitted to the NCBI Sequence Read Archive (SRA) under BioProject n. PRJNA412797 (1B: SRX3362329. 1B_LB: SRX3362328. 1B_LB_D: SRX3362331).

2.5. Analysis of microbial community structure

All 16S rRNA sequences generated in the present study were evaluated for quality using FastQC (Babraham Bioinformatics, 2020) and processed in mothur (Schloss et al., 2009) with trimming of adapters, primers and barcodes. Additional quality control was carried out using the following criteria: maxhomop = 6, maxambig = 0, minlength = 200, qwindowaverage = 30, bdiffs = 1, pdiffs = 2, and tdiffs = 2. Mothur was used to align quality filtered sequences to the SILVA (Quast et al., 2013) database. Chimeric sequences were removed using the mothur implementation of Vsearch (Rognes et al., 2016). QIIME was used for open reference OTU calling and taxonomic assignment of the high-quality 16S rRNA sequences against the SILVA nr v132 release. Taxonomic classification was summarized in QIIME and subsequently visualized in R with ggplot2 (https://scholar.google.co.in/scholar?hl=enamp;as_sdt=0%2C5amp;q=ggplot2+elegant+graphicsamp;btnG=).

2.6. Liquid microbial fuel cells (L-MFCs) and redox potential, O_2 and pH measurements

In order understand microbial electrogenic activity along the water column and to create a bioreactor where it is possible to carry out bioremediation studies in aqueous environments, L-MFCs were built. To obtain a liquid microbial fuel cell (L-MFCs, Logan et al., 2006), gold electrodes were fixed on the wall of the microcosms containing the bacterial solution (cathode). The electrical circuit was completed by a pair of bare gold electrodes or gold needle electrodes immersed above the biofilm grown in the

diesel-water interface (anode). The electrodes were mounted on a micropositioner equipped with micro-adjustment rings (Signatone S-725 micropositioner, Lucas Signatone Corporation, USA) and connected to a multimeter. The redox potential (RP) was determined by placing the electrode of the micropositioner on the biofilm. The surfaces of the immersive bare gold electrodes measured 0,55 cm^2 each. L-MFC set up for 50 mL tube is demonstrated in Supplementary Fig. 1 and Video S1.

An L-MFC prototype was built for this study with a radius of 12 cm and a height of 54 cm, to have easy access to the water column of the microcosm during RP, O_2 and pH measurements. The description is provided in Supplementary Fig. 2 and Video S1. For the evaluation of how the cutting experiment influenced the RP along the water column, a polymethylmethacrylate (PMMA) based L-MFC with a radius of 3 cm and a height of 9 cm was built (Supplementary Fig. 2C, Video S1).

RP measurements were performed at steady state. A custom electronic analyzer dedicated to microbial fuel cells was also used (Pietrelli et al., 2019), to obtain a complete electrical characterization of the L-MFCs. This measurement tool allowed complete electrical characterization of the L-MFCs through analysis of the charge and discharge phases of MFCs, with accurate determination of the values of voltage (V), power density (W/m 2), and current density (A/m 2). The instrument made it possible to carry out cell characterizations using resistive loads in the range between 0 Ω (short circuit measurement) and 10 kΩ (Supplementary Fig. 3). Dissolved oxygen (microprocessor HI 9143, Hanna Instruments, Italy) and pH measurements (HD8602, Delta OHM, Italy) of L-MFC prototype were performed at the beginning (T0) and the sixth month (T6).

2.7. Enrichment of filamentous bacteria from the water column of L-MFC

Bacterial filaments (Fig. 1E) were collected from the water column of the L-MFC prototype. The filaments were pelleted at 300 rcf and gently resuspended in M9. Filaments were smeared on plates with LB agar and incubated at 30°C for 24 h in aerophilic conditions.

To study the bacterial filamentation, single colonies were taken from plates and grown in LB in 15 mL tubes (Falcon) incubating in microventilation conditions at 30°C for 7-10 days at 0 rpm. Preparations were observed continuously with a ProgResC10 optical microscope (Nikon, Italy).

2.8. Scanning (SEM) and Transmission (TEM) electron microscopy

For SEM analysis, floating biofilms (1B_LB_D) were collected from the diesel-water interface and left to adhere on poly-lysine treated glass coverslips for 4 h at RT. Samples were processed as previously described with some modifications (Fassell et al., 1992). Osmium post-fixed samples were dehydrated through a graded series of ethanol solutions. Then ethanol was gradually substituted by hexamethyldisilazane (HMDS) through a 1:1 (ethanol: HMDS) incubation for 30 min, followed by pure HMDS for 1 h and then by a final drying process, totally removing HMDS and leaving to evaporate all the liquid phase under chemical hood for 2 h. On the other hand, the sample enriched of filaments were delicately taken from the water column of the culture tube, left to adhere to poly-lysine treated glass coverslips for 2 h and directly air-dried.

All dried coverslips were mounted on stubs, gold sputtered (10 nm) and analyzed by FE-SEM Quanta Inspect F (FEI - Thermo Fisher Scientific; Eindhoven - The Netherlands).

For TEM analysis, the floating biofilms or the filaments in the water column were fixed in 2,5% glutaraldehyde, 2% paraformaldehyde, 2 mM CaCl2 in 0.1 M sodium cacodylate buffer overnight at 4°C, and were processed as previously described by Perry and Gilbert with slight modifications (Perry et al., 1979). Samples were embedded in Agar 100 resin (Agar Scientific Ltd, Stansted Mountfitchet - England) and ultrathin sections, obtained by a UC6 ultramicrotome (Leica Microsystem, Wetzlar - Germania), were stained with uranyl acetate and Reynolds' lead citrate.

For negative staining, filaments were sampled in the central part of the broth-oil tube culture and deposited on carbon-coated grids, let to adsorb for 20 min and the excess fluid blotted by filter paper. Ammonium molybdate 2% contrasting solution was added and the extra fluid blotted by filter paper after 30 s.

All TEM samples were examined by EM 208S TEM (FEI - Thermo Fisher Scientific; Eindhoven - The Netherlands) at 100 kV, equipped with the Megaview SIS camera (Olympus).

2.9. Mid-Range infrared spectroscopy

To confirm the presence of lipids in the oil-water interface, medium-range infrared spectroscopy was performed at the beginning (T0) and six months (T6) from the inoculation of bacteria in the L-MFCs. The sample was carefully collected at the diesel-water interface just above the biofilm of an electrogenic L-MFC at the sixth month of incubation. Spectroscopy was performed on an Agilent FT-IR Cary 660 (Italy) spectrophotometer with a diamond attenuated total reflection (ATR) sampling interface. The oil samples were cold dried and analyzed without any pretreatment in the spectral range 400-4000 cm^{-1} (Goñi et al., 2006).

2.10. Immunofluorescence, thunder imager 3D cell culture and confocal laser scanning microscopy (CLSM)

Bacterial aggregates in the sample 1B_LB_D were analyzed with a THUNDER Imager 3D Cell Culture (Leica Microsystem, Wetzlar - Germany). Cells were stained in 96-well microplates with 4',6-diamidino-2-phenylindole (DAPI, Thermo Fisher Scientific, Invitrogen) 10 µg/mL for 10 min at room temperature (RT) and quickly examined by using a 40x/0.60 NA objective and a Stage Navigator for Image Stiching at high resolution.

For membrane detection, filaments from the enriched sample were directly stained in the culture plate with DAPI for 10 min at RT, followed by FM1-43 (Thermo Fisher Scientific, Invitrogen) 5 µg/mL for 5 min. Bacterial cells were then seeded on a microscope slide with a broken tip to avoid the breakage of filaments, covered with a cover glass and examined by CSLM. To detect Myelin Basic Protein (MBP) and Claudin 11 (O_4), bacterial cells were collected by centrifugation at 6000 rcf for 15 sec. A small number of bacteria was seeded on a glass slide and fixed with 4% paraformaldehyde for 30 min at RT. Cells were then incubated for 2 h with the oligodendroglia marker O_4 (hybridoma supernatants IgM, custom made, also called Claudin 11) or with different types of anti-MBP antibodies: a mouse monoclonal anti-MBP (1:100, #MAB382, from Chemicon International, USA), a.a. 129-138 (GTLSKIFKL), an anti-Myelin Basic Protein SMI 94R, a.a. 70-89 (PVVHFFKNIVTPRTPPPSQ) from Covance, MA, and a rabbit polyclonal a.a. 102-116 (GGRASDYKSAHKGF) from Sigma-Aldrich, Italy (Bernardo et al., 2017. As secondary antibody, fluorescein-conjugated goat anti-mouse IgM or IgG CyTM3 fluorophore, respectively for O_4 or anti-MBP primary antibodies (1:200, Jackson ImmunoResearch Laboratories, Inc, West Grove, PA) were used. Coverslips were finally mounted with Vectashield Mounting Medium-plus DAPI (Vector Laboratories, Burlingame, CA).

CLSM observations were performed with a LSM980 Zeiss apparatus equipped with Airyscan 2, using a 63x/1.40 NA oil objective and excitation spectral laser lines at 405, 488 and 543 nm. Image acquisition and processing were carried out using the Zeiss Confocal Software Zen 3.0 (Blue edition). Signals from different fluorescent probes were taken in sequential scan settings. Several

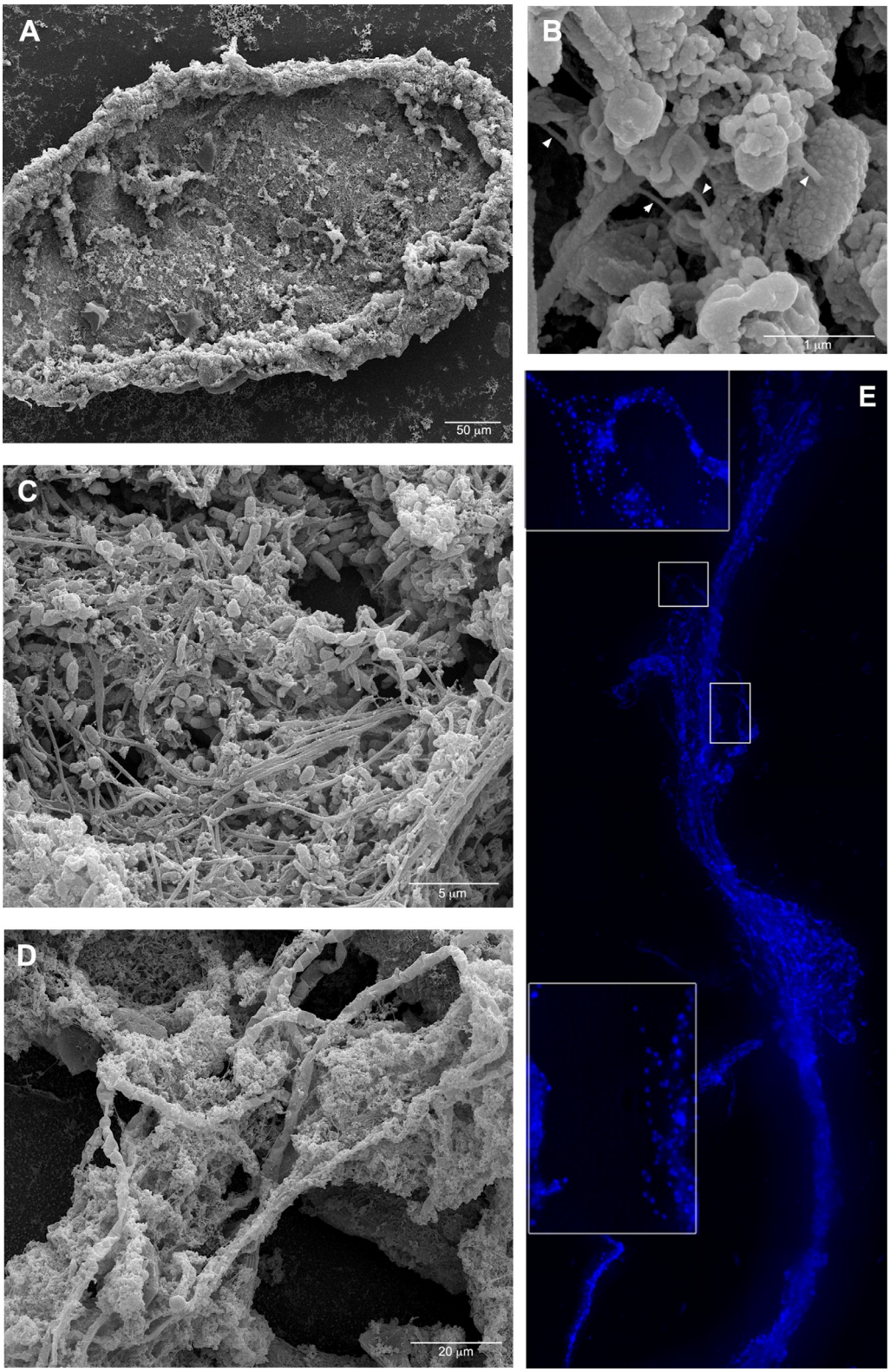

Fig. 1. Hydrocarbonoclastic floating biofilm of a mixed bacterial community cultured in M9/diesel media: from the oil-water interface to the water column. A, SEM micrograph of a floating aggregate of hydrocarbonoclastic bacterial biofilm from oil-water interface; B, the floating biofilm analyzed at high magnification: one type of filamentous bacteria that constitute a sort of irregular biofilm scaffold; C, a different kind of filamentous bacteria composed of barrel-shaped cells contained in a large sheath and connecting thick regions of the floating biofilm (arrows); D, SEM micrograph of the nanowire-like structures that connect bacilli and filamentous bacteria in the biofilm showed in B (head arrows). E, Thunder Imager 3D microscopy analysis of the biofilm filamentous bacteria which extend themselves in a water column, from the oil-water interface (anoxic zone) toward the oxid zone. DAPI was used for DNA detection (blue). Insert shows the oval shaped structures queueing in a ribbon-like envelope.

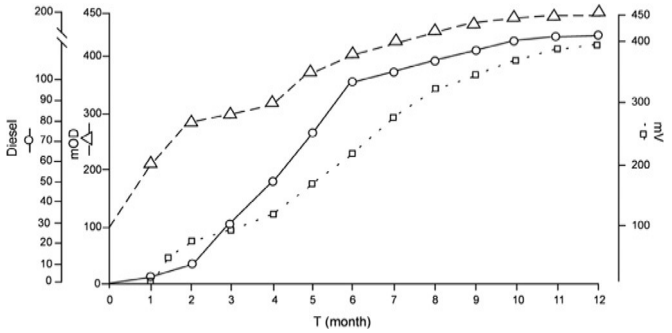

Fig. 2. Hydrocarbonoclastic growth and RP trend of 1B_LB_D sample during the follow-up. Electrical data (mV), hydrocarbonoclastic activity (Diesel: percentage of diesel oil consumed from T0), bacterial growth (mOD: millioptical density at 600nm) during a year of incubation in diesel oil (T0-T12).

filament aggregates were analyzed, and representative results are shown.

2.11. Western blot analysis

For cell-based assay, cells and filaments from the enriched sample were pelleted at 6000 rcf, washed twice in M9 media and lysed in 50 mM TRIS HCl (tris(hydroxymethyl)aminomethane hydrochloride), pH 7.4, 150 Mm NaCl, 0.25% NaDeoxycholate, 1 mM EDTA (ethylenediaminetetraacetic acid), 1 mM EGTA (ethylene glycol-bis(2-aminoethylether)-N,N,N′,N′-tetraacetic acid), 1% TritonX-100, 0.5% IGEPAL (Octylphenoxy poly(ethyleneoxy)ethanol, branched), and protease inhibitor cocktails (Sigma Aldrich, USA) on ice for 30 min. Cell lysates were centrifuged at 4°C at 13000 rcf for 30 min and processed for immunoblotting. Briefly, proteins (100 µg) were separated on 12% SDS-PAGE and transferred to a nitrocellulose membrane (all from Bio-Rad, CA, USA). MBP expression level was evaluated using an anti-MBP monoclonal antibody (#MAB382, Chemicon International, USA). Anti-MBP antibody was also used to differentiate between the endogenous protein from control oligodendrocytes. The results were confirmed in three independent experiments.

3. Results and discussion

3.1. Hydrocarbonoclastic floating biofilm as a mixed bacterial community

Hydrocarbonoclastic bacteria in collected water samples were enriched in microcosms where diesel oil was added as the sole carbon source . This microbial population showed the ability to colonize the static oil-water interface by producing a significant number of floating flock-like aggregates. The growth of this community was analyzed by SEM which showed bacterial cells meshed in a substantial amount of extracellular polymeric substance that contributed, together with cellular debris, in developing this flock-like structures floating on the static oil-water interface (Fig. 1A). Numerous fibrillar elements were also observed in the extracellular matrix and created a rough biofilm scaffold (Fig. 1B) and some more giant filamentous structures composed of barrel-shaped cells contained in a large sheath connecting thick regions of the floating biofilm (Fig. 1C). All these bacterial chains probably provided a tool both for floating and connecting the different parts of the culture from the oil-water interface throughout the underneath water column.

Moreover, numerous nanowire-like connections (40-60 nm in width) were also observed between bacillar bacterial shapes and filamentous bacterial cells in the floating parts of the biofilm

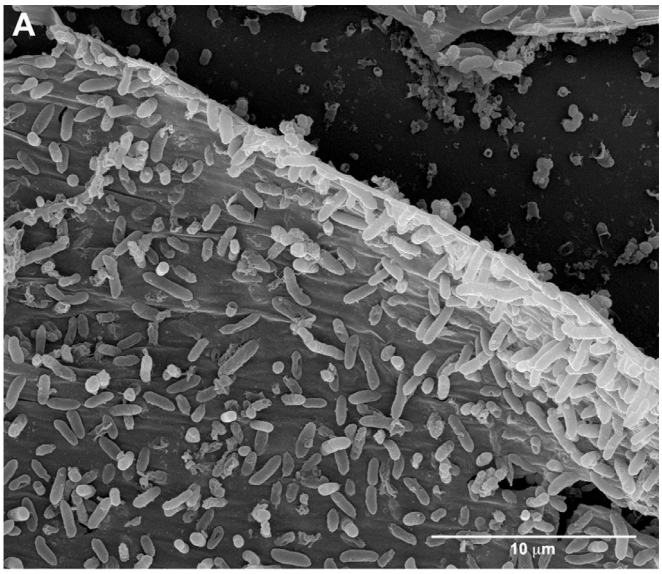

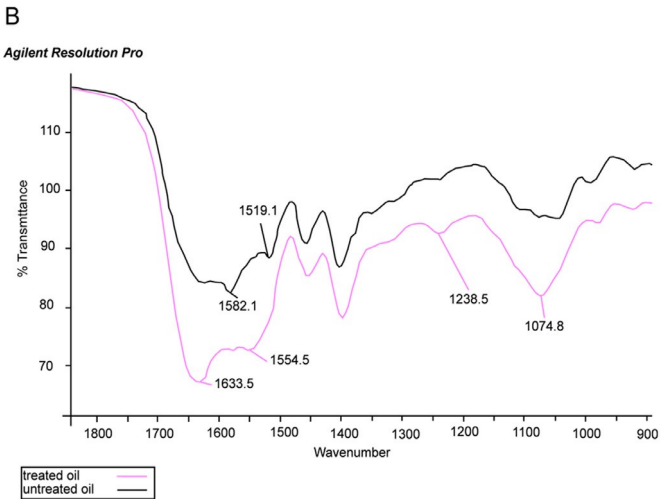

Fig. 3. Surface active compounds analysis. A, SEM image of the membrane at the oil-water interface. **B,** Infrared Spectra of interface before and after biofilm formation showed the presence of an N-acyl sphingosine (ceramides) together with some phospholipids. Spectrum peaks with the corresponding wavelength and chemical group were assigned to: ~1633cm^{-1} (amidic C=O stretching), ~1554cm^{-1} (C-N stretching and N-H in plane bending), ~1238cm^{-1} (P=O stretch), ~1075cm^{-1} (Out-of-phase P-O-C stretch).

(Fig. 1D). In the same cultures, some filamentous bacteria that extended themselves in the water column, from the oil-water level, produced huge strands (more than 500 µm in length) containing DNA detected by DAPI staining (Fig. 1E). At high magnification, these strands were shown as consisting of oval-shaped structures queueing in a ribbon-like envelope (inserts).

3.2. Microbiome

To study the freshwater microbial community at the oil-water interface, environmental sample 1B previously enriched in LB (1B_LB), was immersed in diesel for 12 months. The 16S rRNA gene sequences analysis at the class level for samples 1B, 1B_LB and 1B_LB_D is shown in Supplementary Fig. 4A. At the sixth month, the study of microbial successions showed that in the diesel-immersed sample (1B_LB_D), compared to previous samples 1B and 1B_LB, the whole community (100%) was composed of the

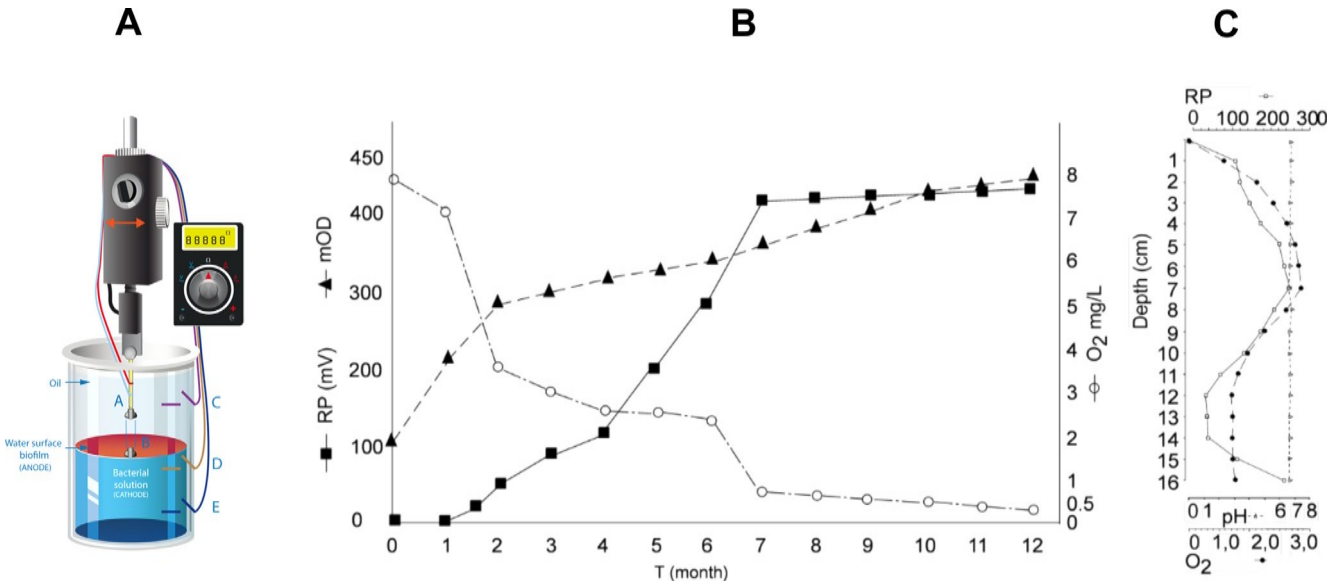

Fig. 4. Liquid-Microbial Fuel Cells. A, shows the L-MFC obtained from falcon tube by introducing gold electrodes on the walls (C, D, E). A micropositioner and a multimeter or other instrument has been used for the detection of redox potential (RP), current (i) and power (W). L-MFC produced current only by placing the electrode of the micropositioner in contact with membrane (position B), while positioning it in diesel did not generate electrical signals (position A). **B**, RPs follow up in L-MFC prototype. The trend for 12 months of redox potential (mV) by placing the cathode at 6 cm from the biofilm is showed. Bacterial density (mOD: millioptical density at 600nm) and O_2 concentration (mg/L) were also measured. **C,** measurements of RP, pH and O_2 along the water column (Depth, cm) of the L-MFC prototype at a sixth month from the bacterial inoculum. (average values, N= 10).

Proteobacteria phylum. More than 97% was represented by the γ-Proteobacteria class and 2.2% by α-Proteobacteria. These microcosms grown in diesel under conditions of microventilation (hypoxic) showed a decrease in biodiversity, as already described in soils contaminated with diesel (Borowik et al., 2018). Phylum like Firmicutes, Actinobacteria, Bacteroidetes and Acidobacteria were absent in the microcosms 1B_LB_D.

The γ-Proteobacteria are a metabolically versatile class of bacteria, including a large number of species present in environments characterized by massive presence of hydrocarbons (Hazen et al., 2010). Some of the best known hydrocarbonoclastic γ-Proteobacteria include *Oceanospirillales, Cycloclasaticus*, and *Halomonas*, and include those that were identified in the Gulf of Mexico during the Deep Water Horizon oil spill (Hazen et al., 2010, Gutierrez et al., 2016). The microbiome analysis at the genus level (Supplementary. Fig. 4B) showed the presence of *Serratia sp., Pseudomonas sp.,* and *Shewanella sp,* which are known hydrocarbon degraders (Wongsa et al. 2004, Wasi et al., 2013, Rathoura et al., 2018). Growth of these facultative anaerobes could be favoured in these oxygen-poor microcosms and could play a role in diesel degradation. The ubiquitous *Shewanella sp.* represented over 80% bacterial abundance in our microcosms; it is known for its ability to conduct electricity and also to promote the electrogenic biodegradation of diesel in microbial fuel cells under anaerobic conditions (Morrisa et al., 2009). The presence of flavin in the *Shewanella sp.* cytoplasm allows the transport of the electrons sequestered in the dehydrogenation of Nicotinamide Adenine Dinucleotide (NADH-NAD)towards the outer membrane (Fonseca et al., 2013). Furthermore, in the outer membrane, the presence of different types of cytochromes c guarantees an RP difference to allow the flow of electrons. Through connection elements called "nanowires", the electrons can pass to adjacent cells to reduce oxygen, heavy metals and other oxidants such as sulphates and nitrates (Pirbadian et al., 2014; Cooper et al., 2003). The presence of nanowires in biofilms has been described as a factor leading to an increase in current in microbial fuel cells designed using *Geobacter sulfurreducens* biofilms (Reguera et al., 2006).

Although the data from this microbiome study confirmed the presence of putative electrogenic bacterial elements such as *Shewanella sp.*, it did not reveal the nature of the filaments observed in the biofilm. This could be due to difficulty in extracting nucleic acids from filaments or due to presence of bacterial genera for which no filamentous forms are known. Bacterial filamentation processes have been described for *Pseudomonas putida* in which oxygen became a limiting factor during growth on a variety of liquid media (Jensen et al., 1985). Similarly, *Serratia sp., Shewanella sp.*, and *Aeromonas sp.*, the latter found only in traces ($< 1\%$), could contribute to the filamentous shape of the biofilm observed in sample 1B_LB_D.

3.3. Liquid microbial fuel cells

3.3.1. Operating L-MFCs

To verify the electrogenicity and hydrocarbonoclastic activity of the microbial community, L-MFCs were supplemented with diesel as the only energy source (Supplementary Figs.1, 2). The electrogenic trend of the microbial community grown in the L-MFCs was analyzed as shown in Fig. 2. Like in other MFCs reported previously (Logan et al., 2006), the anode at the diesel-water interface donated electrons while the underlying cathodic region containing O_2 functioned as an electron acceptor (Supplementary Fig. 1).

3.3.2. Membrane of L-MFCs

Electron microscopy analysis was performed to investigate how the hydrophobic and hydrophilic areas of L-MFC were separated.

SEM micrographs showed the presence of a membrane at the oil-water interface, which could be constituted by a lipid layer that separated diesel from hydrocarbonoclastic bacteria present in the hydrophilic phase (Fig. 3A). Infrared spectroscopic analysis at diesel-water interface showed the formation of an N-acylsphingosine (ceramide) together with some phospholipids (Fig. 3B). These molecules represent surface-active compounds (SAC, Georgiou et al., 1992), which consist of hydrophilic and hydrophobic domains preferably distributed over the interface. They

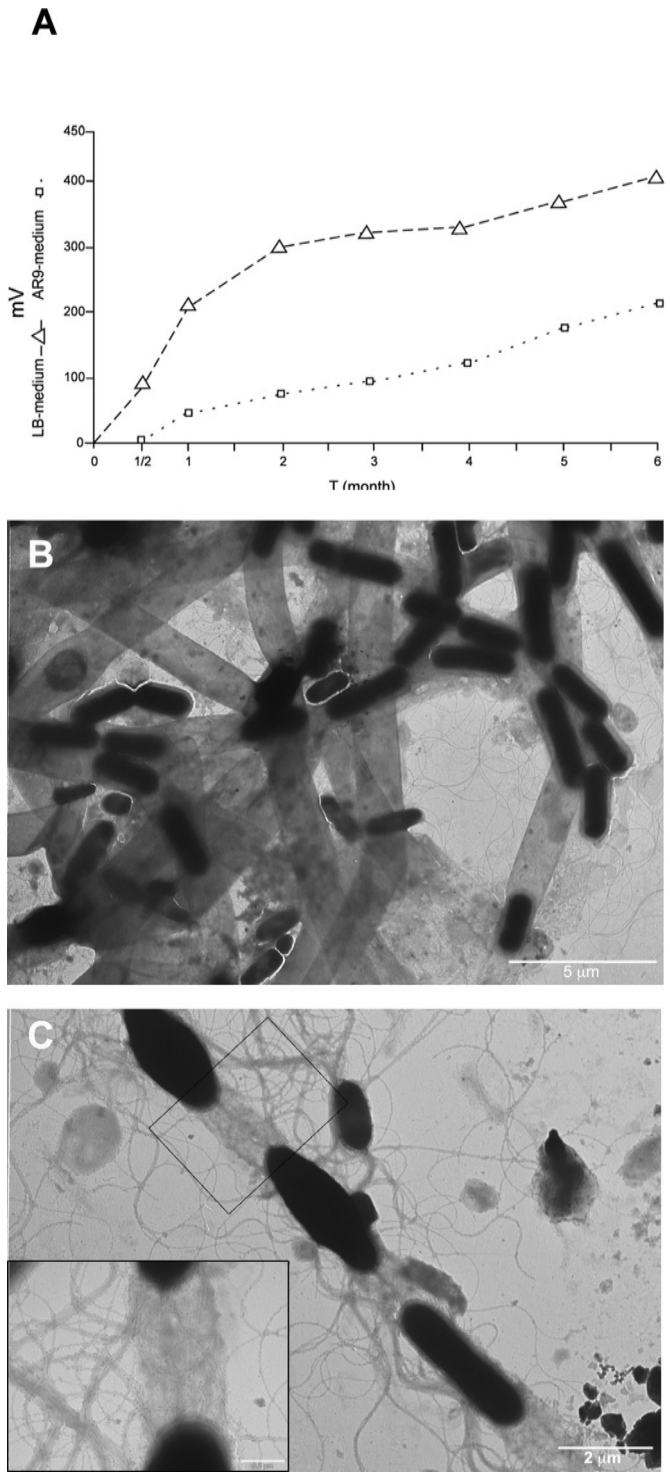

Fig. 5. Enriched colture of filaments from the water column of L-MFCs. A, RPs trend during six months of follow up of the electrogenic enriched colture of filaments in L-MFC tubes set up**.** The growth of the filaments in the batteries was carried out using diesel as the only energy source (small square) and with LB broth (triangle). **B,** TEM negative staining of the filaments from the water column showing their string nature due to bacilli enwrapped into an electron transparent envelope. **C**, Detail of a train of bacilli connected each other by a great number of flagella (insert).

could ensure bioavailability and consequent degradation of hydrocarbons at the interface level, as previously described (Klein et al., 2010).

As shown in Fig. 4A, the L-MFC produced current only by placing the electrode of the micropositioner in contact with this membrane (position B), while positioning it in diesel did not generate electrical signals (position A). This observation suggested that the anodic region of the L-MFC was located on the membrane of the diesel-water interface and that it functioned as a charge separator allowing evocation of RP. Therefore, this kind of L-MFC could represent a natural battery present in the hydrocarbon-water interface, not yet identified until now.

3.3.3. RP, O_2 and pH in L-MFCs

An L-MFC prototype (Supplementary Fig. 2) was built for studying the changes in bacterial growth, biofilm formation and electrogenicity (as RP) with the O_2 variations, using diesel as a sole energy source. Measurements were made at 6 cm from the oil-water interface with carbon electrodes, as described above. In the first two months, an increase of OD could be observed with a reduction in the O_2 concentration that moved from 7 mg/L at T0 to suboxic values of 4 mg/L at T2, when RP and biofilm began to be detected. In the successive months, O_2 trend was opposite to RP decreasing until the 7th month. From this point onwards a maintenance of an electrogenic state was observed, despite hypoxic values of O_2 less than 1 mg/L (Fig. 4B). At month 6, RP, pH and O_2 were also measured all along the water column of L-MFC (Fig. 4C). Maximum values of RP with O_2 at 3 mg/L were observed at 6-7 cm with a peak of 300 mV at the bottom of the battery, where the concentration of O_2 dropped to almost anoxic values (less than 1 mg/L).

These data are in agreement with the characteristics of an electron donor like *Shewanella sp*. or other electrogenic bacteria that use metals as an electron acceptor under conditions of oxygen depletion (Sulu-Gambari et al., 2016; Castro et al., 2014). Although other mechanisms could be involved, the reduction of these acceptors, which could explain the maintenance of RP, was supported by the multitude of crystals observed on the bottom of the L-MFC during the hypoxic and anoxic phases of hydrocarbon degradation (Fig. 4B and Supplementary Fig. 5).

On the contrary, RP was not observed just below the biofilm (2-3 mm) where O_2 was not detectable. RP and O_2 lack were in agreement with the hypothesis of the creation of an anoxic state under the biofilm. The presence of RP immediately after the anoxic zone suggested electrical connections that started from the biofilm and reached the water column (Fig. 4C). The pH trend was almost unchanged throughout the water column around the values of 6.8-7 (Fig. 4C). However, an increase was expected around the oxic area, due to the consumption of protons for water formation ($4H^+ + 4e^- + O_2 \rightarrow 2H_2O$). The pH stability in L-MFC was not analyzed, but its increase was probably counteracted by the forced solubilization of CO_2 and protons released during the oxidation of hydrocarbons.

3.3.4. Filaments and O_2 in L-MFCs

To determine if changes in the RP was due to the presence of a bacterial electrical network observed in the biofilm and the water column, the sample was incubated in an L-MFC equipped with a thin (0.50 mm) blade for cutting of the water column (Supplementary Fig. 2C and Video S1). The steel blade was rotated horizontally through the water column 2-3 mm below the biofilm, thus transiently interrupting the network of bacterial connections. This movement induced a consistent reduction in RP (Supplementary Fig. 6, bar A) which was also obtained by heavily pipetting along the water column (Supplementary Fig. 6, bar B), suggesting that in

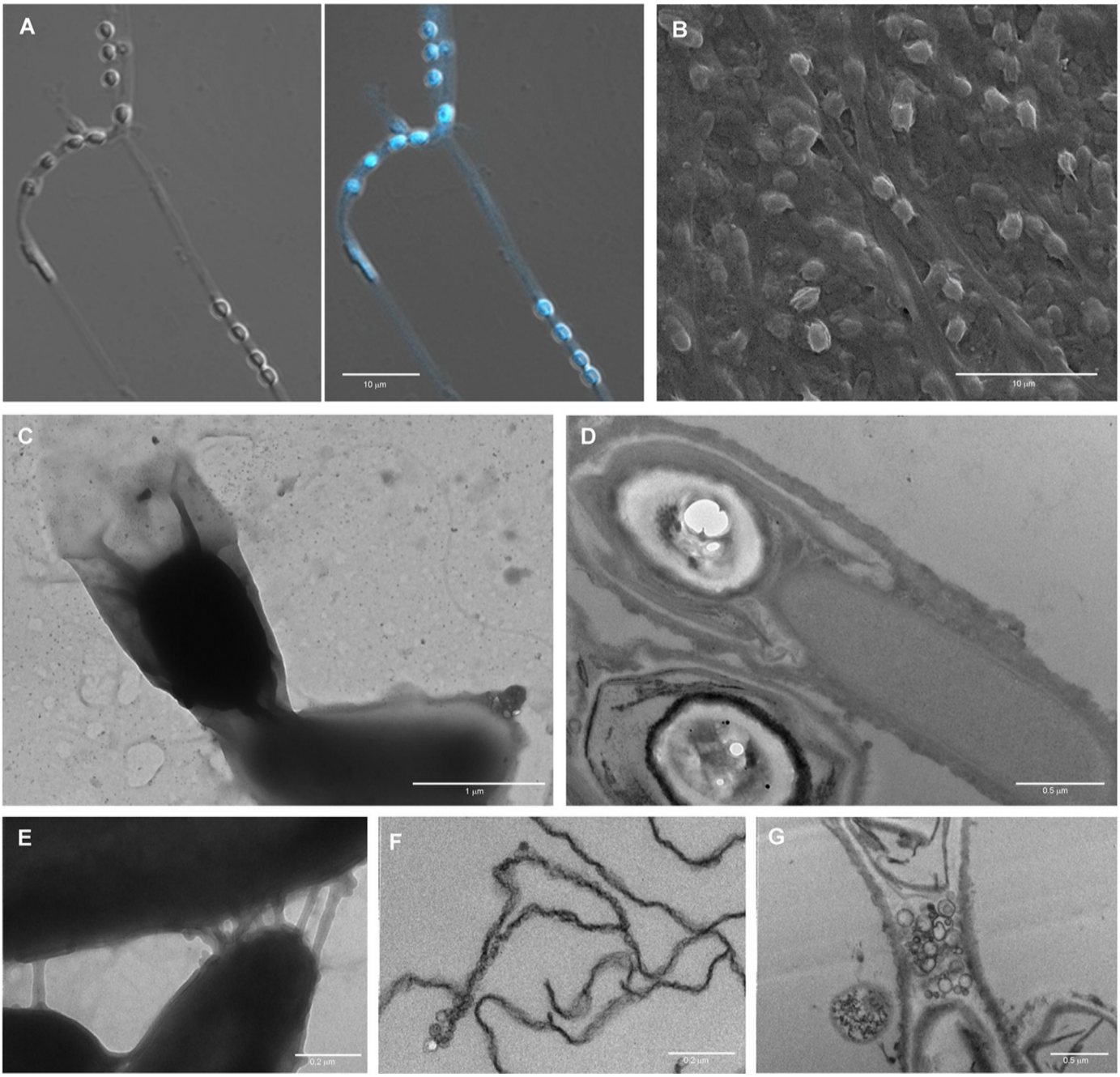

Fig. 6. Ultrastructural analysis of filaments from the water column of an L-MFC. A, Confocal laser scanning microscopy (CLSM) of a discrete bacterial filament in the water column (Nomarsky image overlay with DAPI staining). **B,** SEM micrograph showing the filamentous bacteria organized in a thread of bacilli and spore-like shapes enveloped in a sheath. **C-D,** TEM negative staining and ultrathin section of a bacillus enwrapped with a spore-like shape in the same envelope. **E,** a cluster of bacilli connected by nanowire-like structures (TEM negative staining). **F,** Ultrathin section showing the extracellular nanovesicle chains. **G,** Ultrathin section of the area between two adjacent spores: numerous membrane nanovesicles were present.

the water column there could be a thick component responsible for electron transfer.

Introducing O_2 along the water column up to 6-7 mg/L resulted in a dramatic reduction of RP (Supplementary Fig. 6, bar C). This finding suggested that there was an optimal range of oxygen concentration in L-MFC for RP generation (Fig. 4C). Hypoxic levels of 3-4 mg seemed to favor RP while higher O_2 concentrations reduced it. A shift from an anaerobic phase, with electric current production, to an aerobic phase, without the electric current output of the facultative anaerobic community 1B_LB_D, could explain this result (Supplementary Fig. 4). The accessibility of the biofilm or the filaments along the water column to O_2 could perhaps allow the completion of the catabolic processes and make the activation of microbial electrical connections redundant to transport electrons to O_2 in distant zones.

3.3.5. Ultrastructural analysis of filaments from the water column of L-MFCs

To study the filamentous elements of the L-MFC, enriched culture of filaments from the water column (Fig. 1E) were grown alone using diesel oil as sole energy source. These microcosms were able to form biofilm at the oil-water interface and to produce detectable RP in L-MFC with diesel as sole energy source and

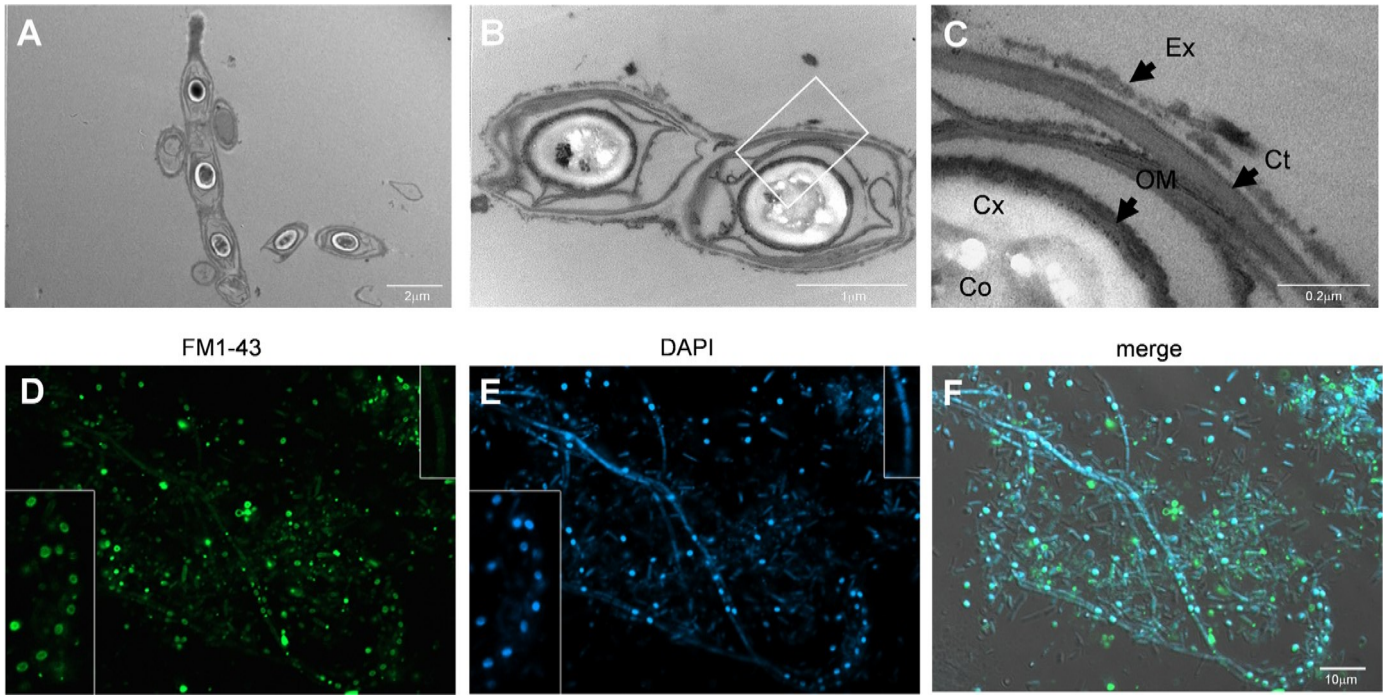

Fig. 7. Multi-lamellar layers in the spores stacked in the filaments developed by the enriched sample from the water column. A-B, TEM micrograph of the filaments showing spore-like structures into filaments: a train of spore-like structures queued in the same shell; C, high magnification of the spore-like layers; Ex: exosporium; Ct: coat; OM; outer membrane; Cx: cortex; Co: core); D-E, CLSM analysis of filaments stained in vivo with FM1-43 (green) and DAPI (blue). Inserts represent higher magnification images showing the bright FM1-43 fluorescence in the spores and the weak signal in the bacilli. Nomarsky image overlay with DAPI and FM1-43 are also shown (F). Panels are representative of 3 independent experiments.

in LB broth (Fig. 5A). Both conditions were optimal for the growth and study of the filaments identified in L-MFCs.

Filaments were morphologically analyzed by electron microscopy, revealing their pleiotropic nature when grown in a hypoxic environment. CLSM and SEM analyses showed bacillar and oval shapes. Both included in a loose tubular structure of several microns in length (Fig. 6A, B). TEM negative staining of filaments confirmed the presence of an electron-lucent tubular structure that wrapped more electron-dense bacillar cells (Fig. 5B). This envelope contained both bacterial cells and a structure resembling bacterial spores (Fig. 6C, D; Rabi et al., 2017).

Interestingly, these spore-like shapes were observed during the drastic reduction of O_2 (< 3 mg/L) after about three months of culture and over, during the maturation of L-MFCs when RP settled at around 400 mV (Fig. 4B). When this filamentous structure was not completely developed it revealed the presence of some complex flagellar connections between bacterial cells, organized to form a string observed in the first two months of incubation of the L-MFCs (Fig. 5C). It is conceivable that these flagella contributed both to the bacterial filament building and to cell-cell electron transfer which in turn could be responsible for one of the potential electrogenic mechanisms in the L-MFCs (Malvankar et al., 2014). However, whatever was involved in the electron transfer process, these shell-wrapped bacilli supported the growth of filaments from the oil-water interface over long distances. Although it was not verified whether the filaments could conduct electrical current, it was likely that they could contribute to the generation of RP in the L-MFC where the filaments were present as the most abundant organisms (Fig. 5A). Besides flagellar filaments, other ultrastructures were observed that could be hypothesized to be responsible for the electron transport at distance. Indeed, bacterial nanowire-like structures derived from the bacilli outer membrane and nanovesicle chains composed by numerous juxtaposed extracellular vesicles (<30 nm in diameter) were observed by TEM (Fig. 6E, F) and SEM (Fig. 1D). These observations were also supported by the microbiome data that showed the presence in this hydrocarbonoclastic biofilm of genera capable of producing nanowires.

Moreover, numerous nanovesicles were also detected in the area between two spore-like structures enclosed in the same envelope (Fig. 6G). They all could be proposed as tools that play a role in RP production (Sure et al., 2016; Subramanian et al., 2017; Ramírez-Flores et al., 2019). The variety of organized structures capable of electron conduction has recently been enriched by the observation that also cytochrome c protein chains in a liquid environment are capable of inducing electron transfer in the absence of vesicles or membranes supporting electron transport without electrical dispersion (Lagunas et al., 2018).

3.3.6. *A myelin-like network for the electrogenic filaments of L-MFCs*

A more detailed TEM analysis has been performed to understand the ultrastructure of these new pleiotropic bacteria when grown in a hypoxic environment. Ultrathin sections showed that the bacterial filaments consisted of trains of oval-shaped structures contained in a coarse shell and displayed all layers usually present in a bacterial spore (Fig. 7A, B). In particular, we observed an inner coat (Ct) characterized by a fine lamellar appearance of multiple membrane layers (> 12 coils) which strongly resembled a myelin-like structure. Under the coat layers, it was possible to discern the outer membrane (OM) of the spore and the cortex (Cx). The inner membrane around the core (Co) was not visible in these ultrathin sections (Fig. 7C). The space between these wrapped spores was often filled by numerous vesicles and membrane coilings, which could be involved in electron transfer (Fig. 6G).

To verify the phospholipid nature of the myelin-like layer, CLSM analysis of filaments was performed with FM1-43, a lipophilic compound usually used for staining of the myelin sheaths of Schwann cells (Nishikawa et al., 2011). Live-labelled samples showed an intense annular signal around the spores in the fila-

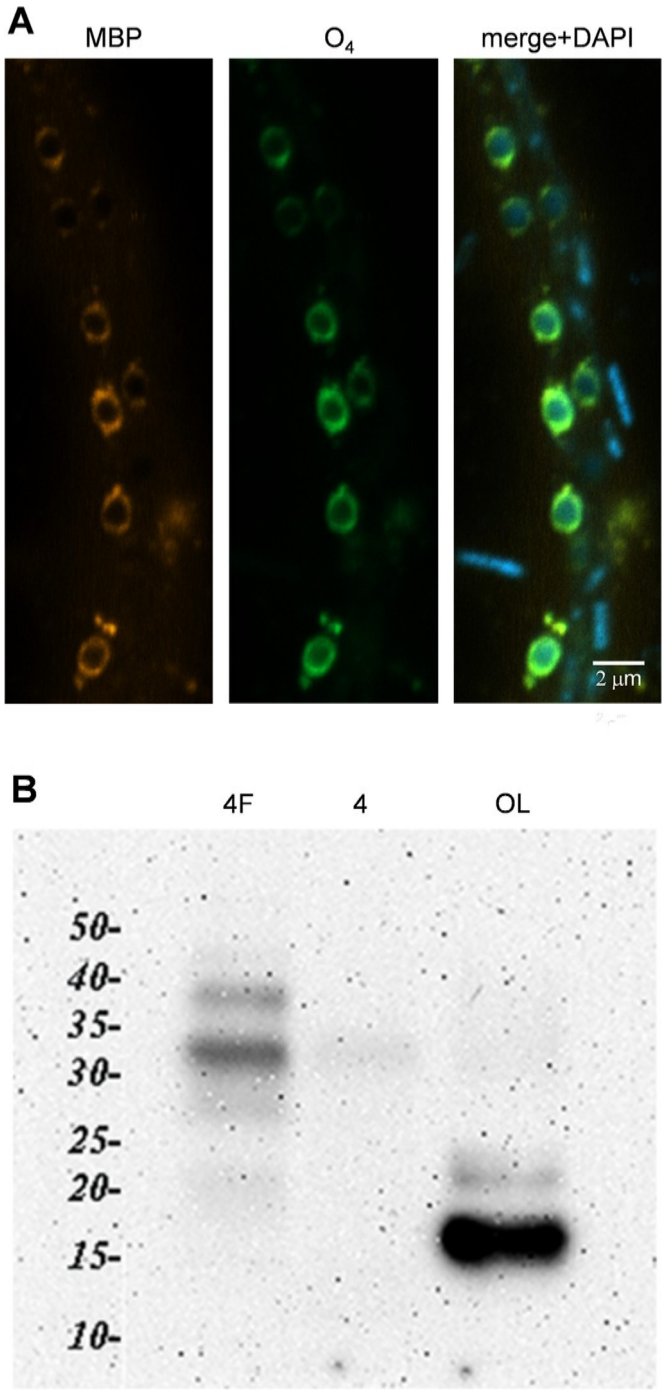

Fig. 8. MBP and O_4 (Claudin 11) detection in myelin-like filaments of the enriched sample. A, CLSM analysis of filaments from the L-MFC water column fixed, permeabilized and stained for MBP (orange) and O_4 (green) detection. DAPI was used for DNA staining (blue). Co-localization of MBP and O_4 proteins is shown in merged images, detected in yellow. **B**, MBP Western Blot on filaments of spores (lane 4F) and bacilli (lane 4) of the enriched sample and on oligodendrocyte control (lane OL). The isoforms of about 35 kDa and 22-23 kDa are shown in the protein extract from the filaments of spores. Representative examples of 3 independent experiments are shown.

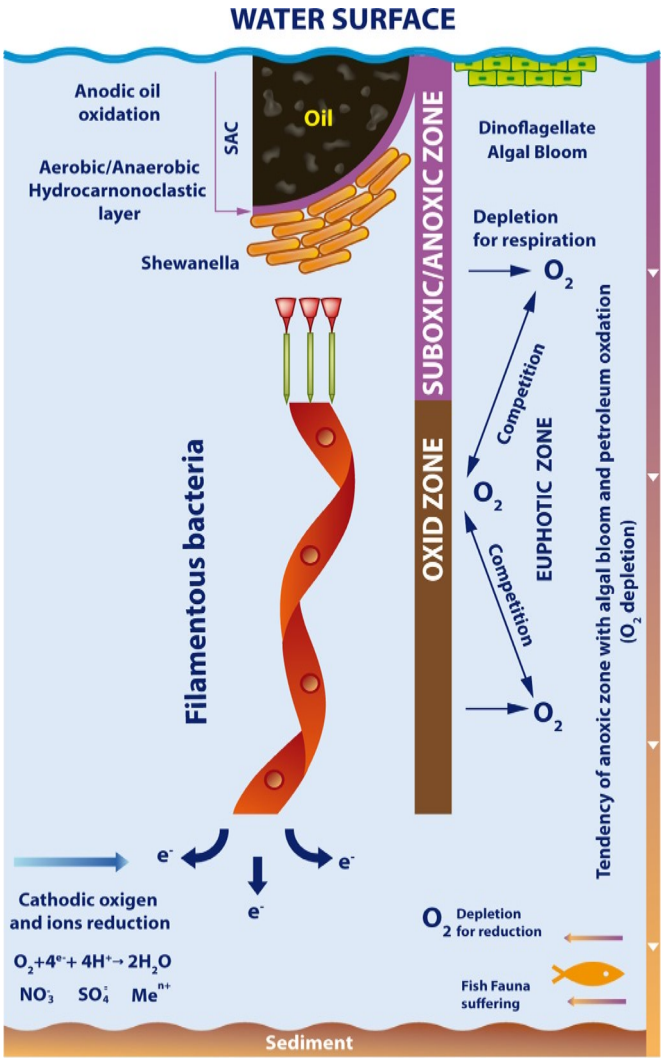

Fig. 9. Model hypothesis for electron transfer through the pelagic microbial community during oil spills and algal bloom in a lake. On the surface of the water (i.e. Pertusillo Lake), the hydrocarbonoclastic biofilm growth and respiration together with dinoflagellate bloom observed, could allow the depletion of O_2 concentration. Furthermore, the presence of these blooms on the water surface would prevent the dissolving of the photosynthetic O_2 produced by algae in the water. The created hypoxic-anoxic environment in the euphotic zone would induce the electronic passage in the water column, likely due to the presence of species such as both *Shewanella sp* and putative electrogenic filaments. Given the respiration properties of these species, acceptors other than O_2 such as heavy metals, sulphates, nitrates or crystal deposits could be involved. The anoxic environment created, together with the chemical pollutants due to oil spills, could lead to further adverse effects also on fish fauna such as those observed in Pertusillo Lake (De Pace et al., 2019). These findings suggest one of the possible mechanisms on how lacustrine microbial communities can cope with oil spills.

ments, probably consistent with the multi-lamellar layers. At the same time, the bacilli string exhibited a much weaker green fluorescence indicative of a lower phospholipid content (Fig. 7D). Furthermore, FM1-43 and DAPI staining of our filaments confirmed their ability in developing peculiar threads in which both bacilli and spores are wrapped to form giant filaments (Fig. 7D-F). This complex filamentous structure thanks to the floating due to the high presence of lipids, could facilitate the connection of the water column to the hydrocarbonclastic biofilm of the L-MFC and could be involved in the RP detected in the water column. Results obtained from the cutting off the water column could support these hypotheses (Supplementary Fig. 6A, B).

These myelin-like structures, entrapped in a unique filament, represented a novel and exciting bacterial feature induced by such challenging environments, deserves further study. They have also been related to structural proteins of oligodendrocytes such as MBP (Boggs et al., 2006), involved in membrane coiling, and O_4 protein. This membrane integrin could be involved in electron transfer (Devaux et al., 2008). The preliminary results (data not

shown) obtained by immunofluorescence for O_4 and three different MBP epitopes (Chou et al., 1986) were followed by CLSM observations and western blot experiments for MBP (Fig. 8). In particular, MBP and O_4 proteins appeared as brilliant ring-shaped fluorescence in the myelin-like lipid multilayer portion, where they co-localized. At the same time, there were no apparent signs for MBP and O_4 in bacillary forms of this bacteria (Fig. 8A). The different degree of MBP expression between these two bacterial forms was confirmed when the "myelinated" filaments were compared with the samples containing only bacillary forms by western blot analysis (Fig. 8B, lane 4F and 4). The sample 4F of filaments having spores, obtained under hypoxic conditions, revealed the presence of MBP epitopes albeit with an isoform pattern different from the MBP of rat oligodendrocytes (Fig. 8B, lane OL). These findings open up exciting scenarios on the action that O_2 depletion exerts on ecosystems and more directly on organisms.

The bacterial filamentation, with the induction of a sort of myelination with multi-layer lipid presence in anoxic environments, could allow the pelagic species to have the advantage of floating along with water column and have a more efficient resistance with the possibility to donate electrons at distance. Furthermore, the multicellularity, the electrogenicity and the cross-reactivity with proteins typical of the nervous system of higher organisms, represent an interesting peculiarity found in these bacteria. The discovery of these “myelinated structures” represents a unicum in the microbial world that has its equivalents in vertebrates and could constitute an example of the common evolutionary project between distant living beings (Morris et al., 2010) that certainly deserves further study.

4. Conclusions

Collectively, our data provide information on oxidative microbial mechanisms during oxygen scarcity triggered by oil spills in a lacustrine ecosystem. Petroleum hydrocarbons stimulated the growth of hydrocarbonoclastic floating biofilms capable of creating organic batteries called L-MFC, with the anodic region in the oil-water interface and the cathodic one along the water column. The presence of hydrocarbons allowed the biofilm to release SAC, generating the spontaneous separation of electrical charges through the oil-water interface. The existence of electrogenic genus such as *Shewanella sp.* could have been responsible for the observed electric current which passed the anoxic barrier under the hydrocarbon-water interface. To complete oxidative processes, the floating filaments could connect the biofilm (anode) to the water column (cathode) thereby facilitating eletcron donation at distance. Given the respiratory preferences of *Shewanella sp.*, acceptors other than O_2 such as heavy metals, sulphates, nitrates or crystal deposits could also be involved (Fig. 9). Our findings therefore suggest a possible mechanism on how lacustrine microbial communities can adapt to oil spills and makes important contributions in enabling better remedial solutions for oil pollution events in lacustrine ecosystems in the future.

Declaration of Competing Interest

The authors declare no competing financial interests.

CRediT authorship contribution statement

Emilio D'Ugo: Conceptualization, Methodology, Writing - original draft, Visualization, Validation, Writing - review & editing. **Lucia Bertuccini:** Writing - review & editing, Visualization, Validation, Data curation, Investigation. **Francesca Spadaro:** Validation, Investigation, Methodology. **Francesca Iosi:** Validation, Investigation. **Fabio Santavenere:** Validation, Investigation. **Fausto Giuliani:** Validation, Investigation. **Massimo Gricia:** Validation, Investigation. **Andrea Rodomonte:** Validation, Investigation, Software. **Nicola Lovecchio:** Validation, Investigation, Software. **Arghya Mukherjee:** Validation, Software. **Paola Bucci:** Validation, Investigation. **Milena Bruno:** Validation, Investigation, Conceptualization. **Emilia Stellacci:** Validation, Investigation, Conceptualization. **Antonietta Bernardo:** Validation, Investigation, Visualization, Conceptualization. **Fabio Magurano:** Supervision, Funding acquisition.

Acknowledgements

We thank Cosimo Curianò and Martina Plebani for their commendable graphics technical assistance; Antonella Marchi, Vittorio Dante and Agnese Brischetto for laboratory assistance. Robert Peter Parker and Melissa Baggieri for the linguistic and critical revision of the manuscript.

Supplementary materials

Supplementary material associated with this article can be found, in the online version, at doi:10.1016/j.watres.2021.117092.

References

ARPAB (Regional Agencies for Environmental Protection of Basilicata) www.arpab.it/risorse_idriche/public/RELAZIONE%20%20PERTUSILLO_Campionamento14marzo2017.pdf (last access 24 sep 2020).

Atlas, RM., 1995. Petroleum biodegradation and oil spill bioremediation. Marine Pollution Bulletin 31, 178–182.

Babraham Bioinformatics, 2020. FastQC source. Bioinformatics Group at the Babraham Institute, UK www.bioinformatics.babraham.ac.uk/projects/fastqc/.

Bernardo, A, Giammarco, ML, De Nuccio, C, Ajmone-Cata, MA, Visentin, S, De Simone, R, et al., 2017. Docosahexaenoic acid promotes oligodendrocyte differentiation via PPAR-γ signalling and prevents tumor necrosis factor-α-dependent maturational arrest. Biochim Biophys Acta Mol Cell Biol Lipids 1862, 1013–1023. doi:10.1016/j.bbalip.2017.06.014, Epub 2017.

Boggs, JM., 2006. Myelin basic protein: a multifunctional protein. Cell Mol Life Sci 63, 1945.

Borowik, A, Wyszkowska, J., 2018. Remediation of soil contaminated with diesel oil. J Elem 23, 767–788. doi:10.5601/jelem.2018.23.1.1583.

Castro, L, Vera, M, Muñoz, M, Blázquez, ML, González, F, Sand, S, et al., 2014. Aeromonas hydrophila produces conductive nanowires. Res Microbiol 165, 794–802.

Chou, CJ, Cox, AA, Fritz, RB, Wood, JG, Kible, RF., 1986. Monoclonal antibodies to human Myelin Basic Protein. Journal of Neurochemistry 46, 47–53.

Cooper, DC, Picardal, FW, Schimmelmann, A, Coby, AJ., 2003. Chemical and biological interactions during nitrate and goethite reduction by Shewanella putrefaciens 200. Appl Environ Microbiol 69, 3517–3525.

De Pace, R, Storelli, MM, Barone, G, Messineo, V, Bruno, M., 2019. Co-occurrence of polychlorinated biphenyls, cyanotoxins and trace elements in commercial fish species from a freshwater protected area (Pertusillo Lake, Southern Italy). Journal of Geography, Environment and Earth Science International 22, 1–14.

Decho, AW., 2000. Microbial biofilms in intertidal systems: 99 an overview. Continental Shelf Research 20, 1257–1273.

Devaux, J, Gow, A., 2008. Tight junctions potentiate the insulative properties of small CNS myelinated axons. J Cell Biol 183, 909–921.

D'Ugo, E, Marcheggiani, S, a D'Angelo A, M, Caciolli, S, Puccinelli, C, Giuseppetti, R, Marcoaldi, R, Romanelli, C, Mancini, L, 2018. Microbiological water quality in the medical device industry in Italy. Microchemical Journal 136, 293–299.

D'Ugo, E, Marcheggiani, S, Fioramonti, I, Giuseppetti, R, Spurio, L, Helmi, K, et al., 2016. Detection of Human Enteric Viruses in Freshwater from European Countries. Food Environ Virol 8, 206–214.

European Parliament 2017, www.europarl.europa.eu/doceo/document/P-8-2017-001300_EN.html?redirect (last access 24 sep 2020).

European Pharmacopoeia 8th edition, 2014. http://www.iss.it/farc/(last access 24 sep 2020).

Fassell, TA, Van Over, JE, Hauser, CC, Buchholy, LE, Edminston, CE, Sanger, JR, et al., 1992. Evaluation of bacterial glycolcalix preseservation and staining by ruthenium red-lysine and alcian blue for several methanotroph and staphylococcal species. Cells Materials 2, 37–48.

Flemming, HC, Wingender, J, Szewzyk, U, Steinberg, P, SA, Rice, Biofilms, Kjelleberg S., 2016. An emergent form of bacterial life. Nat Rev Microbiol 563–575. doi:10.1038/nrmicro.2016.94.

Fonseca, BM, Paquete, CM, Neto, SE, Pacheco, I, Soares, CM, Louro, RO., 2013. Mind the gap: cytochrome interactions reveal electron pathways across the periplasm of Shewanella oneidensis MR-1. Biochem J 449, 101–108.

Georgiou, G, Lin, SC, Sharma SAC, MM, 1992. Surface-active compounds from microorganisms. Biotechnology 10, 60–65.

Goñi, MF, Alonso, A., 2006. Biophysics of sphingolipids I. Membrane properties of sphingosine, ceramides and other simple sphingolipids. Biochimica et Biophysica Acta (BBA) – Biomembranes 1758, 1902–1921.

Gutierrez, T, Berry, D, Teske, A, Aitken, MD., 2016. Enrichment of Fusobacteria in sea surface oil slicks from the deepwater horizon oil spill. Microorganisms doi:10.3390/microorganisms4030024.

Hazen, TC, Dubinsky, EA, DeSantis, TZ, Andersen, GL, Piceno, YM, Singh, N, et al., 2010. Deep-sea oil plume enriches indigenous oil-degrading bacteria. Science 330, 204–208.

Jensen, RH, Woolfolk, CA., 1985. Formation of filaments by Pseudomonas putida. Appl EnvironMicrobiol 50, 364–372.

Klein, B, Bouriat, P, Goulas, P, Grimaud, R., 2010. Behavior of Marinobacter hydrocarbonoclasticus SP17 cells during initiation of biofilm formation at the alkane-water interface. Biotechnology and Bioengineering 105, 461–468.

Lagunas, A, Guerra-Castellano, A, Nin-Hill, A, Díaz-Moreno, I, De la Rosa, MA, Samitier, J, et al., 2018. Long distance electron transfer through the aqueous solution between redox partner proteins. Nat Commun 9, 5157. doi:10.1038/s41467-018-07499-x.

Logan, BE, Hamelers, B, Rozendal, R, Schröder, U, Keller, J, Freguia, S, et al., 2006. Microbial fuel cells: methodology and technology. Environ Sci Technol 40, 5181–5192.

Malvankar, NS, Yalcin, SE, Tuominen, MT, Lovely, DR., 2014. Visualization of charge propagation along individual pili proteins using ambient electrostatic force microscopy. Nature Nanotechnology 9. doi:10.1038/NNANO.2014.236.

Morris, SC., 2010. Evolution: like any other science it is predictable. Phil. Trans. R. Soc. B 365, 133–145. doi:10.1098/rstb.2009.0154.

Morrisa, JM, Jinbc, S, Crimid, B, Prudend, A., 2009. Microbial fuel cell in enhancing anaerobic biodegradation of diesel. Chemical Engineering Journal 146, 161–167. doi:10.1016/j.cej.2008.05.028.

Nishikawa, S., 2011. Fluorescent AM1-43 and FM1-43 probes for dental sensory nerves and cells: their labeling mechanisms and applications. Japanese Dental Science Review 47, 150–156.

Notomista, E, Pennacchio, F, Cafaro, V, Smaldone, G, Izzo, V, Troncone, L, et al., 2011. The marine isolates Novosphingobium sp. PP1Y shows specific adaptation to use the aromatic fraction of fuels as the sole carbon and energy source. Microb Ecol 61, 582–594.

Perry, MM, Gilbert, AB., 1979. Yolk transport in the ovarian follicle of the hen (Gallus domesticus): lipoprotein- like particles at the periphery of the oocyte in the rapid growth phase. J Cell Sci 39, 257–272.

Pietrelli, A, Lovecchio, N, Ferrara, V, Allard, B., 2019. Custom measuring system tailored for MFCs. In: 2019 IEEE 8th International Workshop on Advances in Sensors and Interfaces (IWASI), pp. 270–273.

Pirbadian, S, Barchinger, SE, Leung, KM, Byun, HS, Jangir, Y, Bouhenni, RA, et al., 2014. Shewanella oneidensis MR-1 nanowires are outer membrane and periplasmic extensions of the extracellular electron transport components. Proc Natl Acad Sci USA 111, 12883–12888.

Quast, C, Pruesse, E, Yilmaz, P, Gerken, J, Schweer, T, Yarza, P, et al., 2013. The SILVA ribosomal RNA gene database project: improved data processing and web-based tools Quast C. Nucleic Acids Res 41, 590–596.

Rabi, R, Turnbull, L, Whitchurch, CB, Awad, M, Lyra, D., 2017. Structural characterization of Clostridium sordellii spores of diverse human, animal, and environmental origin and comparison to Clostridium difficile. Spores 2. e00343-17 msphere.asm.org.

Ramírez-Flores, CJ, Cruz-Mirón, R, Mondragón-Castelán, ME, González-Pozos, S, Ríos-Castro, E, Mondragón-Flores, R., 2019. Proteomic and structural characterization of self-assembled vesicles from excretion/secretion products of Toxoplasma gondii. Journal of Proteomics jprot.2019.103490.

Rathoura, R, Guptaa, J, Tyagia, B, Kumarib, T, Thaku, IS., 2018. Biodegradation of pyrene in soil microcosm by Shewanella sp. ISTPL2, a psychrophilic, alkalophilic and halophilic bacterium. Bioresource Technology Reports 4, 129–136.

Reguera, G, Nevin, KP, Nicoll, JS, Covalla, SF, Woodard, TL, Lovley, DR., 2006. Biofilm and nanowire production leads to increased current in Geobacter sulfurreducens fuel cells. Appl.Env.Microbiol 72, 7345–7348.

Rognes, T, Flouri, T, Nichols, B, Quince, C, Mahé, F., 2016. VSEARCH: a versatile open source tool for metagenomics. PeerJ 4, e2584 eCollection.

Schloss, PD, Westcott, SL, Ryabin, T, Hall, JR, Hartmann, M, Hollister, EB, et al., 2009. Introducing mothur: open-source, platform-independent, community-supported software for describing and comparing microbial communities. Appl Environ Microbiol 75, 7537–7541.

Subramanian, P, Pirbadian, S, El-Naggar, MY, Jensen, GJ., 2017. The ultrastructure of Shewanella oneidensis MR-1 nanowires revealed by electron cryo-tomography. PNAS doi:10.1073/pnas.1718810115.

Sulu-Gambari, F, Seitaj, D, Meysman, FJR, Schauer, R, Polerecky, L, Slomp, CP., 2016. Cable bacteria control iron-phosphorus dynamics in sediments of a coastal hypoxic basin. Environ Sci Technol 50, 1227–1233. doi:10.1021/acs.est.5b04369, Epub 2016 Jan 14.

Sure, S, Ackland, M L, Torriero, AAJ, Adholeya, A, Kochar, M., 2016. Microbial nanowires: an electrifying tale. Microbiology 162, 2017–2028.

Wasi, S, Tabrez, S, Ahmad, M., 2013. Use of Pseudomonas spp. for the bioremediation of environmental pollutants: a review. Environ Monit Assess 185, 8147–8155.

Williams, DW, Mann, KH., 2020. Inland water ecosystem. Encyclopædia Britannica, inc https://www.britannica.com/science/inland-water-ecosystem.

Wongsa, P, Tanaka, M, Ueno, A, Hasanuzzaman, M, Yumoto, I, Okuyama, H., 2004. Isolation and Characterization of Novel Strains of Pseudomonas aeruginosa and Serratia marcescens Possessing High Efficiency to Degrade Gasoline, Kerosene, Diesel Oil, and Lubricating Oil. Curr Microbiol 49, 415–422. doi:10.1007/s00284-004-4347-y.